Metals and Materials International (2021) 27:5258–5267
https://doi.org/10.1007/s12540-020-00789-4

Galvanic Coupling Effect on Pitting Corrosion of 316L Austenitic Stainless Steel Welded Joints

Amina Sriba[1] · **Jean-Bernard Vogt**[2]

Received: 3 May 2020 / Accepted: 11 June 2020 / Published online: 13 July 2020

Abstract
The aim of this work is to display the effect of the chemical composition of the filler metal (ER316LN and ER308LN) on the corrosion resistance of 316L austenitic stainless steel welded joints, performed using GTAW process. The redistribution of chemical elements from the base metal and from the filler metal in the fusion zone during the welding operation produces a variation in the microscopic structure along the welded joint. The latter comprises distinct microstructural zones identified as fusion zone, fusion line (partially melted zone), heat affected zone, and the unaffected base metal with their own electrochemical response. Our results revealed that the base metal constitutes the anodic region in the welded joint, while the fusion zones behave as the cathodic part protected against corrosion. From the electrochemical corrosion tests, it is concluded that the welded joint 316L/ER308LN exhibits a better resistance to pitting corrosion than the welded joint 316L/ER316LN, but is less resistant to corrosion by dissolution.

Keywords Fusion Zone · Filler Metal · Galvanic Corrosion · GTAW · Potential Corrosion · Pit

1 Introduction

Austenitic stainless steels owe their corrosion resistance to the presence of a high chromium content (typically above 16 wt%) in their chemical composition. It forms a protective oxide layer at the surface, called passive film, which acts to reduce their dissolution rate when immersed in a corrosive environment. For applications in severe environments, 300-serie grades are preferred and their compositions are often fine-tuned to the intended end use. For instance, to overcome pitting, which is the most common form of localized corrosion that occurs in this family of stainless steels; particularly when they are exposed to solutions containing halide ions such as chlorides and bromides, molybdenum is added.

These alloys are mostly weldable by all conventional processes, especially the Gas Tungsten Arc Welding (GTAW) process. Welding involves different parameters that must be carefully monitored, in order to guarantee welded joints with good performance [1–4]. These parameters include voltage, current, welding speed, shielding gas composition, filler metals, etc. In the welded joint, the fusion zone is the most critical area, which is susceptible to undergo corrosion failures. As for the matrix, chromium, molybdenum, and to a lesser extent, nickel are the main elements that can improve pitting corrosion resistance of welded austenitic stainless steels under specific conditions [2]. During welding, several parameters can affect the pitting corrosion resistance of austenitic stainless steels, especially in solutions containing chloride ions. The effect of GTAW parameters on pitting corrosion resistance of austenitic stainless steels has been widely studied [5–9]. According to I. Berenjani et al. [7], the pulsed current causes a decrease in the heat input and an increase in the cooling rate during welding. This promotes finer grains with more delta ferrite in the fusion zone, and leads to more segregation of chromium and molybdenum within this phase. Cyclic potentiodynamic polarization tests have shown that the fusion zone obtained with pulsed current exhibits higher pitting corrosion resistance than that obtained with direct current. Under both conditions, pitting corrosion resistance of the fusion zone is better than that of the base metal. This has been correlated with the presence of

✉ Amina Sriba
amina.sriba@gmail.com

[1] Corrosion, Protection and Durability of Materials Division, Research Centre in Industrial Technologies (CRTI), P.O. Box 64, 16014 Cheraga, Algiers, Algeria

[2] Univ. Lille, CNRS, INRA, Centrale Lille, UMR 8207, UMET – Unité Matériaux Et Transformations, 59000 Lille, France

delta ferrite phase formed in the base metal due to the separation of the alloying elements. Dadfar et al. [8] specified that alloying elements diffusion is impaired during GTAW process due to high cooling rate. Since these elements in the fusion zone are uniformly distributed, delta and gamma phases have the same chemical composition, so that the presence of delta ferrite in the microstructure does not affect the corrosion resistance of the material.

The microstructure of the fusion zone is different from that of the base metal. This is mainly due to the chemical composition variation caused by the mixture of the base metal and the filler metal in the fusion zone during welding. Therefore, the choice of filler metal is of a great importance. It should have the same characteristics as the base metal. These include metallurgical properties and those of corrosion resistance. The use of a highly alloyed filler metal with respect to the base metal would result in a better corrosion resistance of the fusion zone compared to that of the base metal. It is appropriate, on the other hand, to control the extent of this chemical composition variation in these zones, because the selected filler metal can premeditatedly create a galvanic difference between them.

The variation of chemical composition and microstructure in the fusion zone (FZ), the heat affected zone (HAZ), and the base metal (BM) result in electrochemical potential differences resulting in galvanic corrosion between them. This form of corrosion reaching the welded austenitic stainless steels have been amply studied and is involved whatever the welding process; such as microplasma arc weld [10] or arc plasma weld [11–14]. The corrosion rate of the welded joint increases due to the galvanic effect as compared to the non-welded 316L stainless steel, which forms the anode part of the galvanic pair [10]. It corrodes while the fusion zone of the welded joint remains protected against corrosion throughout the temperature range studied. Due to the existence of three different zones, several galvanic pairs [BM/HAZ], [BM/FZ], and [HAZ/FZ] arise. As pointed out by Sánchez-Tovar et al. [12], the fusion zone in an arc plasma welded joint remained protected, while the base metal doubled and tripled its corrosion rate when coupled with the heat affected zone and the fusion zone respectively. However, depending on the process conditions and environment, opposite behaviour of the fusion zone can be observed. The galvanic corrosion resistance of 316L welded joints performed with micro-plasma process [13, 15] was attributed to the presence of delta ferrite phase emerged in the fusion zone near the base metal side.

Taking into account the welded joint properties and the required performance in service, the choice of the filler metal for the welding operation is considered a crucial factor for controlling the chemical composition of the fusion zone. For this reason, it is important to match the filler metal as closely as possible to the base metal. In this paper, the corrosion resistance of 316L welded joints performed by the gas tungsten arc welding process is studied. The work aims at analysing the impact of the difference in the chemical composition of two filler metals, ER316LN or ER308LN, on the corrosion resistance of the welded joints and to investigate the galvanic corrosion phenomenon occurring in the welded joint. The corrosion behaviour of the different zones in the welded joint was studied by analysing Tafel curves and those of anodic polarization in a 3.5% NaCl water solution. The characterization of the corroded surfaces was carried out by scanning electron microscopy (SEM).

2 Experimental Details

2.1 Materials

The base metal used in this study is a commercial sheet of austenitic stainless steel 316L. The filler metals investigated are ER316LN and ER308LN, in the form of rods of 1.6 mm in diameter. Their chemical composition was determined using optical emission spectrometry technique is given in Table 1.

All materials fulfil the AISI standard. ER316LN filler is close to BM 316L but exhibits higher amount of nickel, nitrogen, molybdenum, and chromium than the base metal BM 316L. ER308LN mainly differs from ER316LN by a lower molybdenum and nitrogen content, but a slightly higher chromium content.

These materials have been investigated in their received state, without further heat treatment. The base metal also did not receive any solution heat treatment. Its microstructure (Fig. 1) contained approximately 4% of delta ferrite and the grain size was about 50 µm.

Table 1 Chemical composition of the base metal and the filler metals (wt%)

Material	C	Si	Mn	P	S	Cr	Mo	N	Ni	Co	Cu	Fe
BM 316L	0.0246	0.367	0.988	0.0306	0.001	16.6	1.99	0.0595	10.6	0.0811	0.46	bal.
ER316LN	0.0209	0.300	1.23	0.0191	0.026	18.3	2.45	0.237	12.7	0.0283	0.117	bal.
ER308LN	0.0220	0.287	1.68	0.0129	0.025	19.9	0.0431	0.122	11.2	0.0426	0.0486	bal.

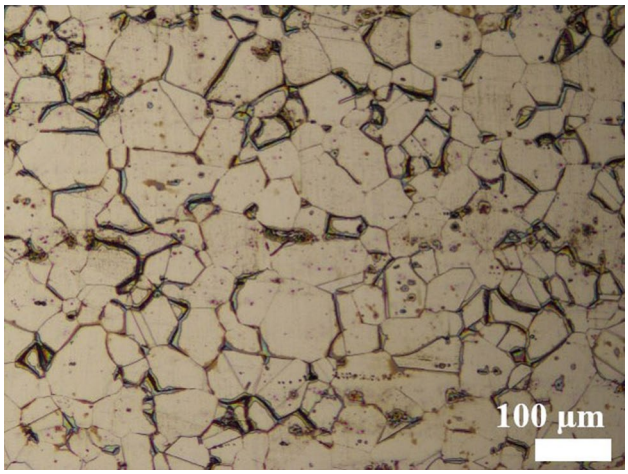

Fig. 1 Optical micrograph of the base metal 316L

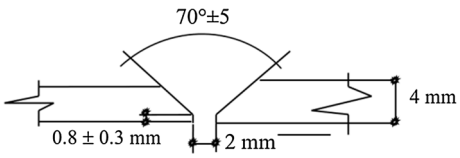

Fig. 2 Butt joint configuration

Table 2 Welding parameters

Welded joint	Current (A)	Voltage (V)	Heat input (kJ/mm)	Welding speed (cm/s)
316L/ER316LN	80–90	9–11	0.29	0.96
316L/ER308LN	80–90	9–11	0.28	0.91

2.2 Welding Operation

Two plates of [500 × 250 × 4] mm have been cleaned with acetone prior to welding operation in order to remove all traces of grease, oil, and oxides. The welding operation was carried out manually using GTAW process in the flat position. The filling of the joint was done in three passes. The configuration of the butt joint is shown in Fig. 2. The shielding gas used was a mixture of argon (~ 96%) and hydrogen (~ 4%) with a flow rate of 11L/min.

The welding parameters are given in Table 2.

The welded joints have been controlled by X-ray radiography. No defects were found on the radiographic films (Fig. 3).

Additional details of the mechanical behaviour the welded joints can be found in [16].

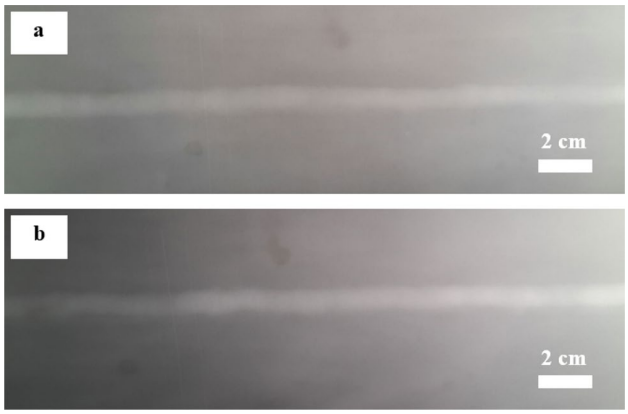

Fig. 3 Radiographic X-ray films of the 316L/ER316LN (**a**) and 316L/ER308LN (**b**) welded joints showing the absence of defects

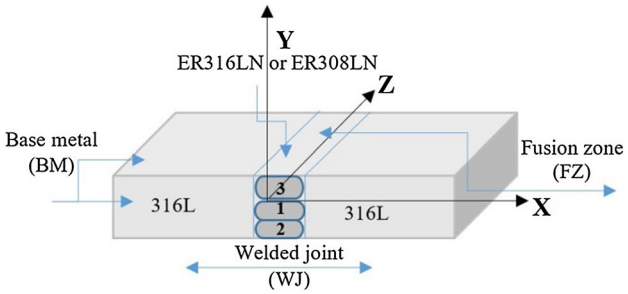

Fig. 4 Diagram showing sample zones for corrosion tests

2.3 Microstructural Characterization

The microstructure along the welded joint was imaged by optical microscopy (Nikon Eclipse LV 100 ND). The electrolytic etching solution used was composed of 90 mL of methanol and 10 mL of chlorhydric acid.

2.4 Corrosion Tests

Corrosion tests have concerned three zones in the welded joint: the base metal (BM), the fusion zone (FZ), and the entire welded joint (WJ). Small pieces of material were cut along the plane [yx] with dimensions depending on the material: 4 × 10 mm for BM, 4x4 mm for FZ, and 28 × 4 mm for WJ, as shown in the diagram presented in Fig. 4.

Corrosion behaviour of these samples was evaluated by Tafel and anodic potentiodynamic polarization methods.

Once a piece of material (base metal, fusion zone or welded joint) was extracted from the weld, an electrical wire was attached. Then the sample was resin molded for further polishing with SiC waterproof paper up to grit 4000 and finally cleaned with alcohol. The testing cell uses a three-electrode configuration where the mounted specimen

Table 3 Chemical composition of the fusion zones of the two welded joints (wt%)

Material	C	Si	Mn	P	S	Cr	Mo	N	Ni	Cu	Fe
BM 316L	0.0246	0.367	0.988	0.0306	< 0.0005	16.6	1.99	0.0595	10.6	0.46	bal.
FZ (316L/ER316LN)	0.022	0.492	1.355	0.029	0.013	16.566	2.341	0.0400	9.408	0.518	bal.
FZ (316L/ER308LN)	0.025	0.380	1.537	0.024	0.012	18.28	0.970	0.0299	9.612	0.305	bal.

constituted the working electrode. The reference electrode and the counter electrode were a saturated calomel electrode (SCE) placed 25 mm from the specimen and platinum electrode respectively. Electrochemical measurements were carried out using a Voltalab PGZ100 potentiostat in a calm solution of 3.5% NaCl without agitation. Before each test, the studied sample was left one hour for an open circuit potential (OCP) measurement in the 3.5% NaCl water solution until its potential has been stabilized.

The potentiodynamic current–potential curves were recorded in the potential range of ±250 mV from the open circuit potential at a scanning rate of 1.667 mV/s. The electrochemical tests were repeated four to five times for each sample in order to ensure reproducibility of the results.

The corroded surfaces were examined with the Quanta 400 FEI scanning electron microscope.

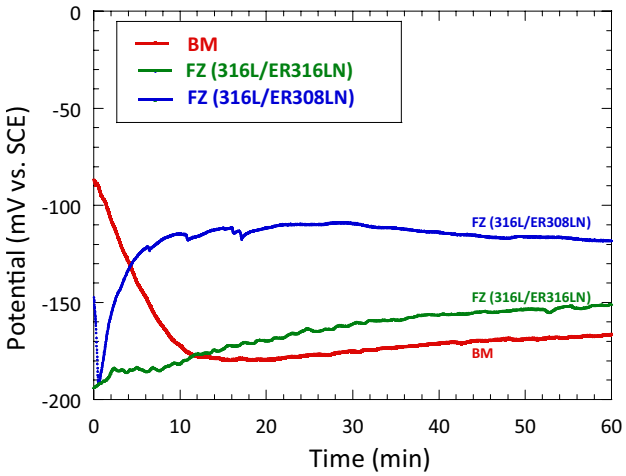

Fig. 5 OCP-time curves for the base metal and the fusion zones

3 Results and Discussion

3.1 Chemical Composition of the Fusion Zones

After welding of the base metal plates with the filler material, the resulting solidified material contained mixed chemical elements of both base metal and filler metal.

Table 3 gives the chemical composition of the fusion zone obtained with each filler metal.

As shown, the fusion zone in the welded joint 316L/ER308LN is now enriched in molybdenum but depleted in nitrogen.

3.2 Corrosion Behaviour of the Base Metal and of the Fusion Zones

Corrosion potential variation provides information on the various modifications and degradations occurring at the interface (metallic surface/electrolyte) of the sample when it is immersed in a corrosive medium. The evolution of open circuit potential versus time of the base metal and of the two fusion zones extracted from the welded joints are presented in Fig. 5.

It is clear that the potential level of the fusion zone (316L/ER308LN) is maintained at higher values, around − 118 mV, compared to that of the base metal BM and the fusion zone (316L/ER316LN). Free potential of the base metal and that

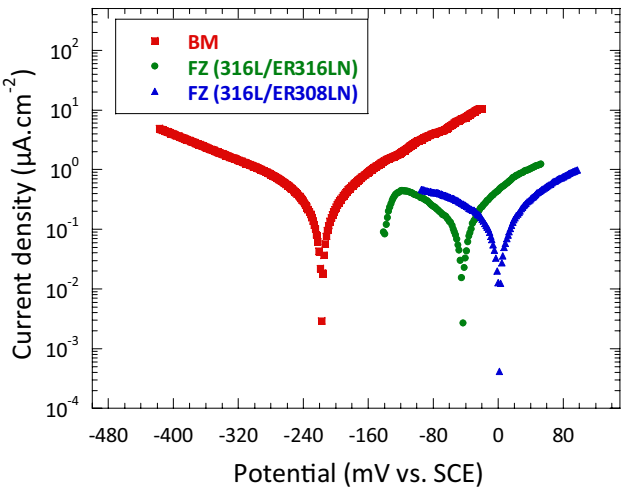

Fig. 6 Tafel polarization curves for the base metal and the fusion zones

of the fusion zone (316L/ER316LN) tend to stabilize to close values. This behaviour is explained by the presence of a passive layer enriched with alloying elements as molybdenum at the surface of the weld metal (316L/ER308LN).

Figure 6 shows Tafel curves of the base metal (BM) and of the two fusion zones (FZ). The cathodic branches of the three curves evolve towards the negative domain of potential. This could be explained by a rapid dissolution occurring

on the metallic surface due to its first contact with the corrosive medium.

The electrochemical parameters deduced by Tafel method are given in Table 4.

Both fusion zones exhibit a higher corrosion potential than the base metal (Table 4); however, the use of ER308LN as a filler metal displaces the corrosion potential of the fusion zone towards much higher values (E_{corr} = 2 mV/SCE) than that of the fusion zone obtained with ER316LN as a filler metal (E_{corr} = -43 mV/SCE). Potential values are related to the alloy chemical composition. In the case of the fusion zone obtained with ER308LN as filler metal, the high corrosion potential is attributed to its high content of chromium (Table 3).

The base metal being the least noble sample with the lowest corrosion potential (E_{corr} = − 217 mV/SCE) is expected to form the anodic part in the galvanic pair (base metal zone/fusion zone), and material of both fusion zones are expected to be the cathodic area in the welded joint. Inversely to the cathodic area where the electrochemical reduction reactions take place, the anodic area constitutes the zone of the electrochemical oxidation reactions. The anode is corroded in favour of the cathode. In the welded joint, the fusion zone has the smallest area compared to that of the base metal. This is the suitable case for a galvanic pair; small cathode area and large anode area. As a result, the risk of initiating pitting, crevice, or intergranular corrosion of this galvanic cell remains relatively low compared to the risk of initiation in welded joints with different size [17].

The high value of corrosion current density of the base metal (Table 4) compared to those of fusion zone may result from an active dissolution of some heterogeneities (ferrite, precipitates, inclusions) in the alloy during potentiodynamic polarization. Indeed, as mentioned above, the base metal has been welded in the as-received state without any annealing treatment. Such effect of initial heterogeneities on the corrosion resistance has been reported by Dadfar et al. [8] in 316L austenitic stainless steel welded by TIG welding process and tested in 0.9% NaCl physiological medium. The better corrosion resistance of the fusion zone was explained by the miss of a secondary phase present initially in the base metal.

It is widely known that localized corrosion occurs at zones containing structural heterogeneities. For example, pitting corrosion of austenitic stainless steels is often associated to non-metallic inclusions present in their structures. The inclusion cleanliness of steels determines generally their resistance to pitting corrosion. The study of non-metallic inclusions role in pitting initiation constitutes the oeuvre of many scientific researchers. The behaviour of the material toward this type of degradation is governed by two parameters. First, the expansion ratio of the matrix and inclusions and second, the thermodynamic stability of these inclusions. Solubility of inclusion is therefore governed by its thermodynamic stability in the medium; it would go into solution and would then be soluble by anodic character initiating a pit. On the other hand, if the inclusion is cathodic, it causes a local dissolution of the surrounding alloy and generates pits [18]. The characterization by SEM–EDS [19] of 316L stainless steel revealed the presence of more than 80 types of inclusions, classified according to their size and density. These inclusions are mainly silicon and other oxides classified in three categories: oxides (Mg–Al), oxides (Mg–Si), and oxides (Ca–Ti–Ce). They have low contents of chromium and molybdenum and a lower surface potential than that of the matrix which makes the passive film weak around them. Usually, pit initiation mechanism near the inclusion is divided into two stages; inclusion dissolution followed by the breakdown of the passive film under the effect of chloride ions (Cl^-) adsorption phenomenon on the surface passive layer [20]. The active process of the inclusion dissolution is located at the interface (matrix/inclusion). It gives rise to an increase in the corrosion current density. Based on these results, it is possible to attribute the rise in corrosion current density of the base metal to the dissolution of inclusions present in the alloy. The latter have either a spherical (Fig. 7a) or elongated (Fig. 7b) shape as pointed out on fracture surfaces after charpy test [16].

3.3 Corrosion Behaviour of the Base Metal and of the Welded Joints

The curve of open circuit potential versus time of the welded joints and the base metal are given in Fig. 8.

The free potential (E°) decreases swiftly during the first minutes of immersion, and then begins to hold steady after about 20 min of immersion in the 3.5% NaCl water solution. This behaviour is explained by a corrosive attack of the alloy surface followed by an electrochemical

Table 4 Electrochemical parameters of the base metal BM and the fusion zones FZ

Materials	E_{corr} (mV/SCE)	Corrosion current density (µA/cm^2)	Polarisation resistance (kohm.cm^2)	Corrosion rate (µm/y)
BM	− 217	0.39	76.8	4.6
FZ (316L/ER316LN)	− 43	0.13	137.2	1.5
FZ (316L/ER308LN)	2	0.18	114.4	2.1

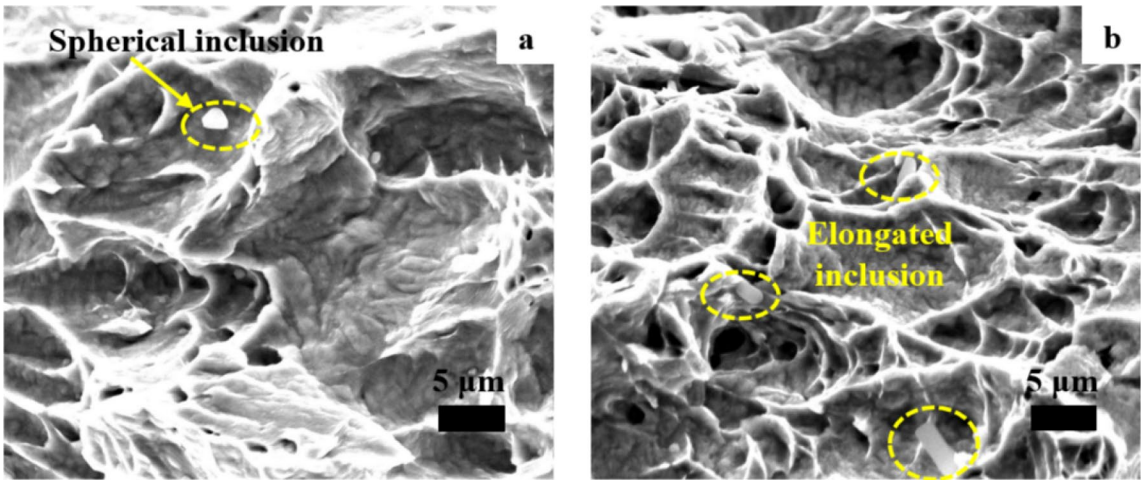

Fig. 7 SEM micrograph showing the presence of spherical (**a**) or elongated (**b**) shape inclusions in the studied materials

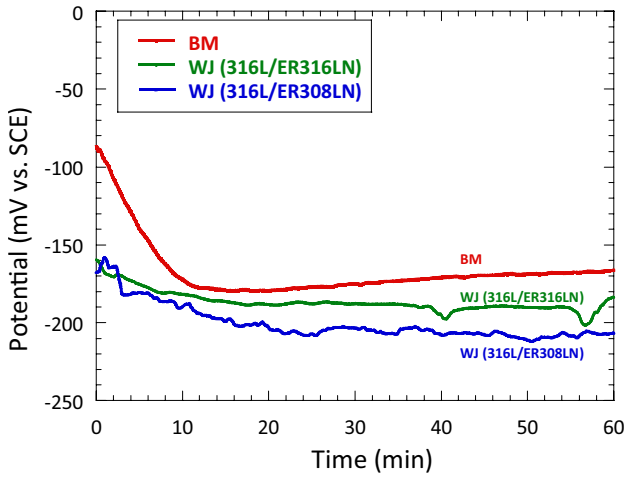

Fig. 8 OCP-time curves for the base metal and the welded joints

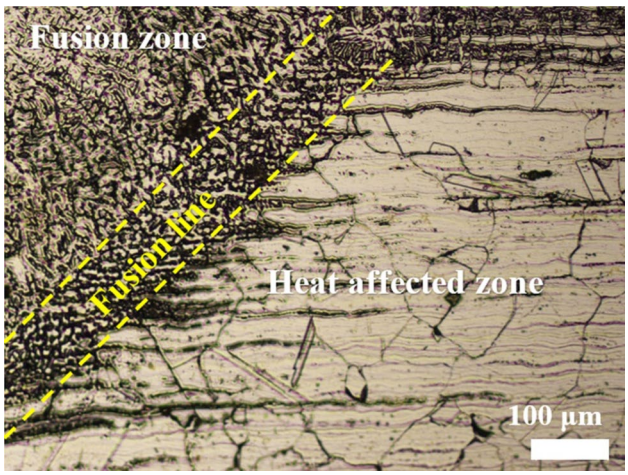

Fig. 9 Optical micrograph showing the fusion line in the welded joint (316L/ER308LN)

equilibrium of the interface (alloy surface/electrolyte). The open circuit potential of the welded joint (316L/ER308LN) stabilizes at slightly lower negative values compared to that of base metal and the welded joint (316L/ER316LN).

Unlike the base metal, which exhibits heterogeneities at the microstructure scale, the welded joint is heterogeneous both at the microstructure and specimen scales and contains different zones; each one having an electrochemical behaviour different from that of the other adjacent zone. Indeed, the welded joint consists of a consecutive assembly of the base metal (BM), the heat-affected zone (HAZ), a fusion line (FL), and finally the fusion zone (FZ) as shown by the optical micrograph of Fig. 9. This causes electrochemical interactions when the entire welded joint is immersed in the 3.5% NaCl solution.

The heterogeneous welded joints are characterized by a corrosion potential less noble than that of the base metal (Fig. 10).

The ranking, in terms of corrosion potential between the weld joints, is just the opposite of that shown in fusion zones. While the fusion zones of both welded joints (316L/ER316L and 316L/ER308LN) had higher corrosion potential values than the base metal BM (Table 3), the welded joints WJ (316L/ER308LN) and WJ (316L/ER316LN) have a lower corrosion potential value than the base metal (Table 5). In addition, the corrosion rate of the welded joint (316L/ER316LN) is lower than the welded joint (316L/ER308LN) (Table 5).

The assembly of all these different components of the welded joints results in higher corrosion current densities than the fusion zone materials and the base metal (Table 4).

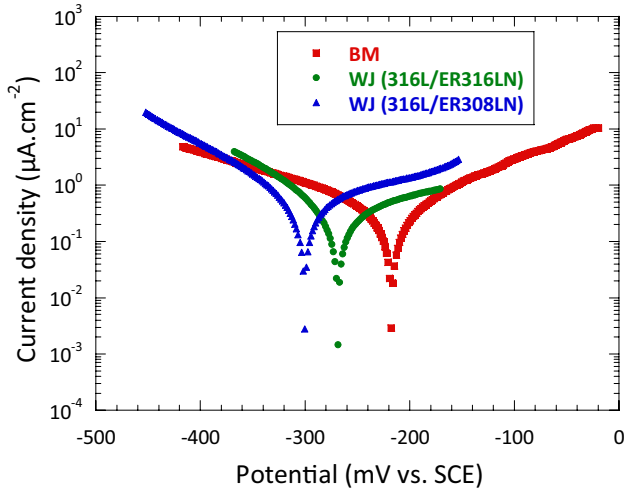

Fig. 10 Tafel polarization curves of the base metal and the welded joints

The fusion line (FL) located between the fusion zone (FZ) and the heat affected zone (HAZ) in the welded joint (Fig. 9) is composed of two parts. One of these consists of a portion of the base metal that had been melted, but mechanically unmixed with the filler metal. The second part is a portion of the base metal partially melted and mixed with the filler metal during the welding operation. The chemical composition of the unmixed zone is the same as that of the base metal, but with a microstructure of an autogenous weld. Its width depends on the local thermal conditions along the weld bead. Micro-segregation and precipitation in the autogenous zones might be preferentially attacked when the welded joint is exposed to a corrosive medium [21]. As a result, they decrease the corrosion resistance of the unmixed zones compared to the base metal.

On the other hand, the heat-affected zone (HAZ) contains coarse grains caused by the heat input during the welding operation.

The difference in the microstructure of the base metal, the heat affected zone, and the fusion line produces potential variations between them when the welded joint is immersed in a corrosive medium. Therefore, a galvanic current would be established between the anode zone and the cathode zone in the welded joint. Its magnitude would be affected by the potential difference between the anode and cathode zones.

Figure 11 shows the anodic polarization curves recorded for the welded joints in the 3.5% NaCl solution. Compared to the behaviour of the base metal, the welded joints exhibit a higher pitting potential than that of the base metal. A passivity zone is observed on all the curves below the pitting potential value. The current density increases sharply at potentials higher than the pitting potentials due to the breakdown of the passive film in the studied samples.

The welded joint obtained with ER308LN filler metal has the highest pitting potential value (188 mV) compared to the welded joint 316L/ER316LN (100 mV) and that of the base metal (90 mV). This behaviour could be the result of the high content of chromium in its fusion zone of the welded joint (Table 3). Thus, it is interesting to note that despite a value of the corrosion density current, the welded joint 316L/ER316LN exhibits a high value of pitting potential (E_{pit}).

3.4 SEM Analysis of Surfaces After Anodic Polarization

Figures 12 and 13 show the SEM micrographs of the different zones in the welded joints (316L/ER316LN) and (316L/308LN) respectively after anodic polarization. These micrographs show the localized attack at their surfaces.

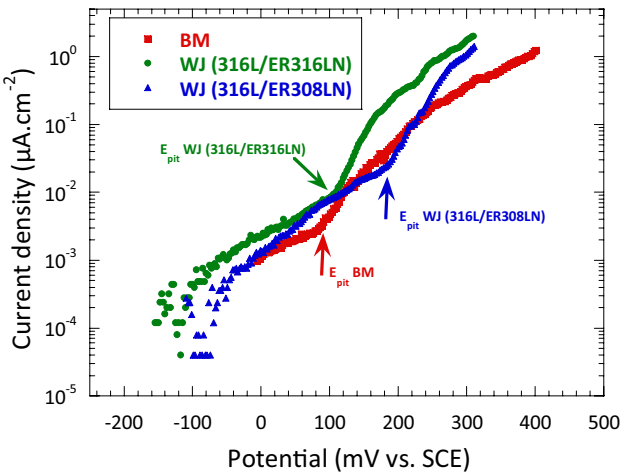

Fig. 11 Anodic polarization curves for the base metal and the welded joints

Table 5 Electrochemical parameters of the base metal and the welded joints

Material	E_{corr} (mV)	Corrosion current density (µA/cm^2)	Polarization resistance (kohm.cm^2)	Corrosion rate (µm/y)
BM (xy)	− 217	0.39	76.8	4.6
WJ (316L/ER316L)	− 268	0.47	73.2	5.5
WJ (316L/ER308L)	− 301	0.59	46.7	6.8

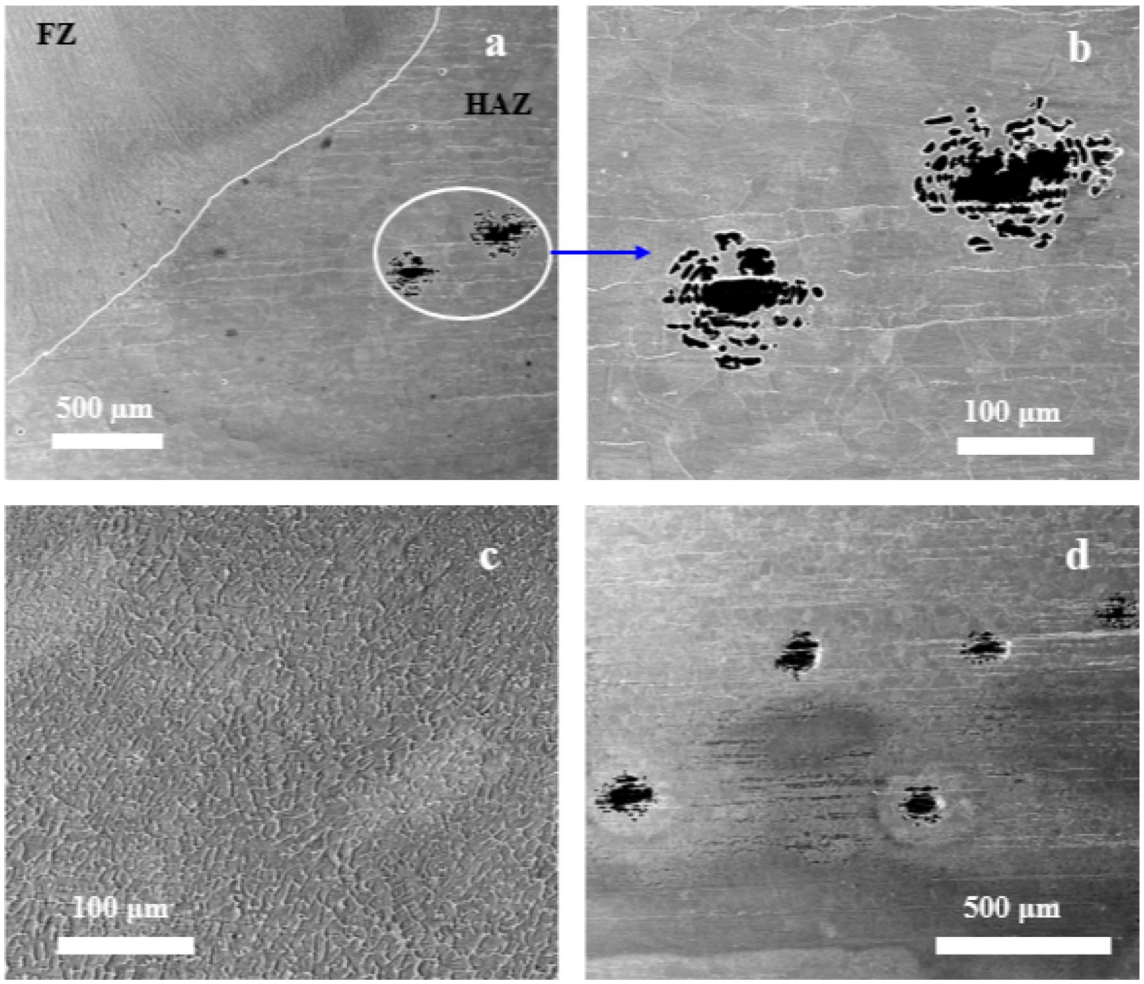

Fig. 12 SEM micrographs of the welded joint (316L/ER316LN) after anodic polarization showing (**a**) the boundary between the fusion zone (FZ) and the heat affected zone (HAZ), (**b**) pits in the heat affected zone,(**c**) the fusion zone free of pits and (**d**) the base metal containing pits

As already concluded from the Tafel curves, the fusion zone constitutes the cathodic part with respect to the base metal playing the role of the anode in the welded joint. The micrographs show that the base metal is severely attacked compared to the fusion zone in both welded joints.

4 Conclusions

The study focused on the corrosion resistance of a welded joint of 316L processed by GTAW by taking into account two different filler metals; ER308LN and ER316LN.

The following conclusions can be drawn:

1 The use of ER308LN as a filler metal leads to corrosion potential value of the fusion zone of the welded joint higher than that of the fusion zone obtained with ER316LN filler metal.
2 Both fusion zones (FZ) have higher corrosion potentials than that of the base metal (BM), but lower corrosion rates and constitute the cathodic part of the galvanic couple (FZ/BM).
3 The welded joint 316L/ER308LN exhibits a better resistance to pitting corrosion than the welded joint 316L/ER316LN, but is less resistant to corrosion by dissolution.
4 The strong difference in the corrosion rate between the base metal and the fusion zones of the welded joint vanishes when the base metal is compared to the welded joint.
5 The initial composition of a filler material for the welding of 316L cannot be considered as the only parameter to control the corrosion resistance of the welded joint.

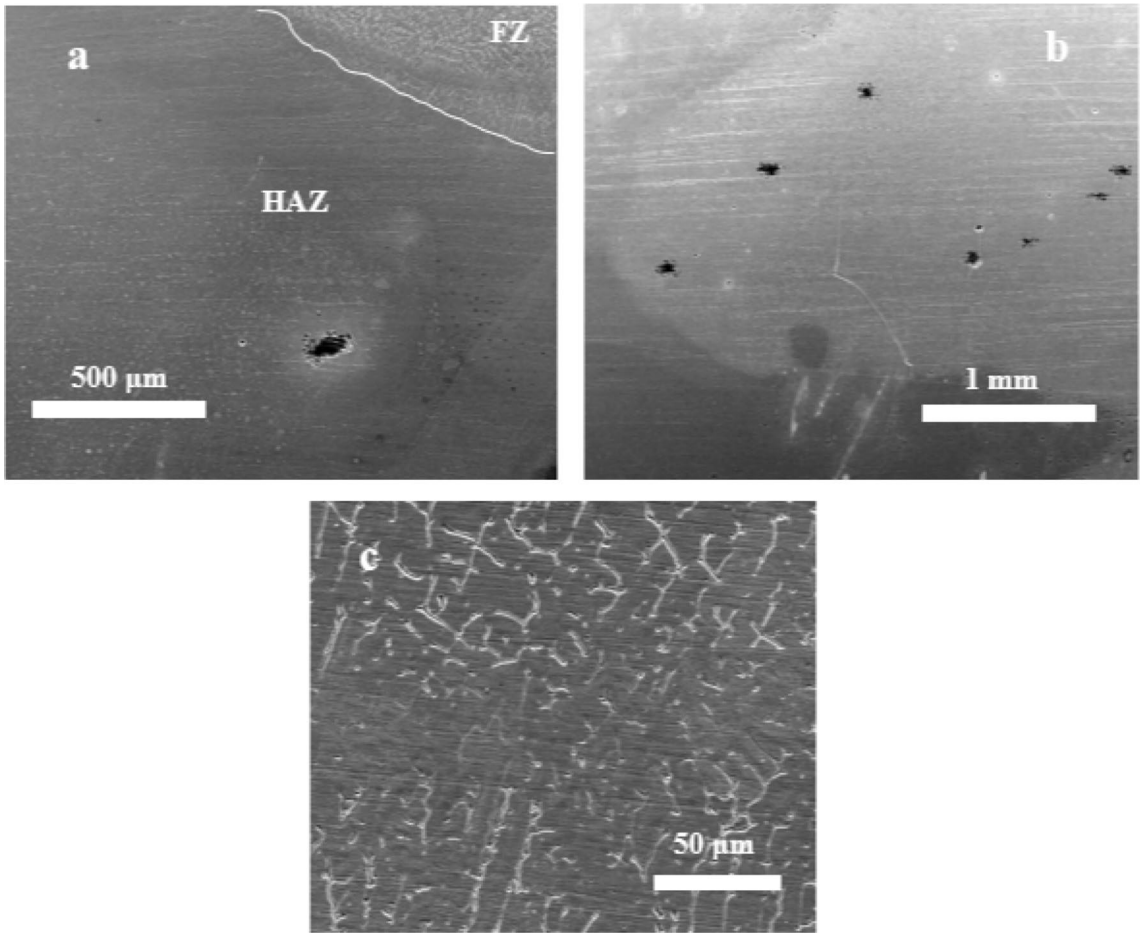

Fig. 13 SEM micrographs of the welded joint (316L/ER308LN) after anodic polarization showing (**a**) pitsin the heat affected zone (HAZ), (**b**) the base metal containing pits and (**c**) the fusion zone free of pits

Authors' Contributions Both authors contributed to the study conception and design. Material preparation, data collection and analysis were performed by Dr. Amina SRIBA. Results analysis were performed by Dr. Amina SRIBA and prof. Jean-Bernard VOGT. The first draft of the manuscript was written by Dr. Amina SRIBA and both authors commented on previous versions of the manuscript. Both authors read and approved the final manuscript.

Funding The research was supported by the institute of each author.

Compliance with Ethical Standards

Conflicts of interest The authors declare that they have no conflict of interest

Ethics The authors declare that the results have not yet published elsewhere.

References

1. G.R. Mohammed, M. Ishak, S.N. Aqida, Metals (2017). https://doi.org/10.3390/met7020039
2. U.K. Mudali, M.G. Pujar, in *Corrosion of Austenitic Stainless Steels Mechanism, Mitigation and Monitoring*, ed. by H.S. Khatak, B. Raj (Woodhead Publishing Limited, Cambridge, 2002), p. 74. https://doi.org/10.1533/9780857094018
3. T.P.S. Gill, U.K. Mudali, V. Seetharaman, J. Gnanamoorthy, Effect of heat input and microstructure on pitting corrosion in AISI 316L submerged arc welds. Corros. Sci. **44**, 511 (1988)
4. F. Muhammad, A. Ahmad, A. Farooq, W. Haider, J. Mater. Eng. Perform. (2016). https://doi.org/10.1007/s11665-016-2240-z
5. P. Paulraj, R. Garg, Eng. Sci. Technol. (2016). https://doi.org/10.1016/j.jestch.2016.01.013
6. R. Sudhakaran, P.S. Sivasakthivel, S. Nagaraja, K.M. Eazhil, Procedia Eng. (2014). https://doi.org/10.1016/j.proeng.2014.12.281

7. I. Berenjani, A. Bakhtiari, K. Raeissi, M. Shamanian, A. Saatchi, Improved pitting corrosion resistance of S. S 316L by pulsed current gas tungsten arc welding. Chem. Mater. Res. **6**, 35 (2014)
8. M. Dadfar, M.H. Fathi, F. Karimzadeh, M.R. Dadfar, A. Saatchi, Mater. Lett. (2007). https://doi.org/10.1016/j.matlet.2006.09.008
9. W. Chuaiphan, L. Srijaroenpramong, J. Mater. Process. Technol. (2014). https://doi.org/10.1016/j.jmatprotec.2013.09.025
10. R. Sánchez-Tovar, M.T. Montañés, J. García-Antón, A. Guenbour, A. Ben-Bachir, Corros. Sci. (2011). https://doi.org/10.1016/j.corsci.2010.12.017
11. R. Sánchez-Tovar, M.T. Montañés, J. García-Antón, Corros. Sci. (2010). https://doi.org/10.1016/j.corsci.2009.12.023
12. R. Sánchez-Tovar, M.T. Montañés, J. García-Antón, Corros. Sci. (2011). https://doi.org/10.1016/j.corsci.2011.04.019
13. R. Sánchez-Tovar, M.T. Montañés, J. García-Antón, Corros. Sci. (2013). https://doi.org/10.1016/j.corsci.2013.04.025
14. C.T. Kwok, S.L. Fong, F.T. Cheng, H.C. Man, J. Mater. Process. Technol. (2006). https://doi.org/10.1016/j.jmatprotec.2006.03.128
15. L.Q. Han, G.B. Lin, Z.D. Wang, H. Zhang, F. Li, L. You, Rare Met. Mater. Eng. (2010). https://doi.org/10.1016/S1875-5372(10)60086-0
16. A. Sriba, J.-B. Vogt, S.-E. Amara, Trans. Indian Inst. Met. (2018). https://doi.org/10.1007/s12666-018-1362-4
17. L. Reclaru, R. Lerf, P.Y. Eschler, J.M. Meyer, Biomaterials (2001). https://doi.org/10.1016/S0142-9612(00)00185-X
18. B.N. Popov, *Corrosion Engineering—Principles and Solved Problems* (Elsevier B.V., Amsterdam, 2015), pp. 290–321
19. J. Liu, T. Zhang, G. Meng, Y. Shao, F. Wang, Corros. Sci. (2015). https://doi.org/10.1016/j.corsci.2014.11.018
20. S. Zheng, C. Li, Y. Qi, L. Chen, C. Chen, Corros. Sci. (2013). https://doi.org/10.1016/j.corsci.2012.09.044
21. J.R. Davis, *Corrosion of Weldments* (ASM International, Materials Park, 2006), pp. 53–54